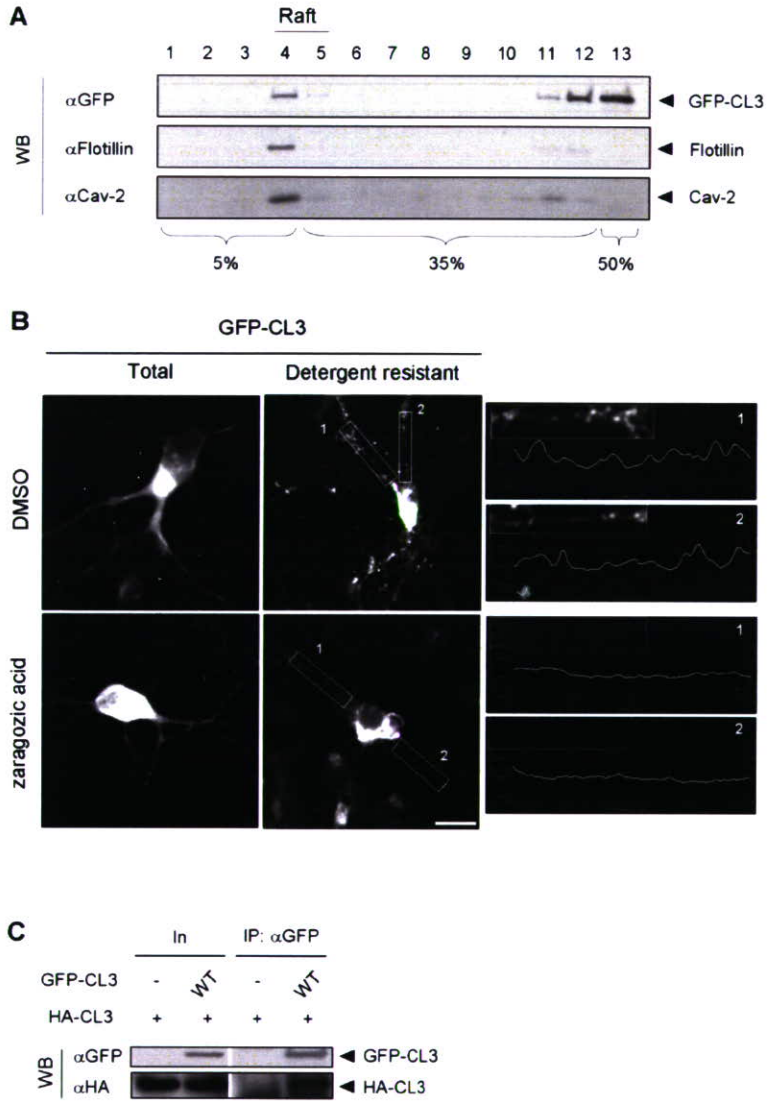

Figure 2. Dendritic Raft Targeting and Multimeric Complex Formation of CL3 in Cortical Neurons

(A) Wild-type GFP-CL3 (WT) expressed in cortical neurons using a synapsin I promoter-driven lentivirus was recovered in the lipid raft fraction (lanes 4–5), as confirmed by the enrichment of raft marker proteins flotillin-1 and caveolin-2 (Cav-2). Fractions 1–4, 5% sucrose; 5–12, 35% sucrose; 13, 50% sucrose.

(B) A sizable portion of total GFP-CL3 fluorescence was recovered after detergent treatment as detergent-resistant GFP-CL3, which was localized in a punctate manner in 2 DIV cortical neurons along the dendrites as well as at the perinuclear region. Dendrites were unambiguously identified as processes of limited length (much shorter than the axon exceeding 100 μm). Line scans of pixel fluorescence, carried out within a chosen field of a 15 μm dendritic segment (in insets 1 and 2) by horizontally tracking the clusters of GFP-CL3, illustrate the spotty presence of raft-inserted CL3 along the dendrites (right panels). Treatment with 100 μM zaragozic acid abolished the dendritic detergent-resistant patches and flattened the line scan profile. Scale bar, 10 μm.

(C) CL3 forms a multimeric complex in cortical neurons. Wild-type CL3 tagged with either HA-tag (HA-CL3) or GFP (GFP-CL3) were coexpressed in cortical neurons by nucleofection and coimmunoprecipitated using an anti-GFP antibody. In, input; IP, immunoprecipitates.

inhibitor of squalene synthase that efficiently depletes membrane cholesterol (Figure 2B, lower panel). These results indicated that CL3 was a genuine component of dendritic lipid rafts and that raft insertion was likely regulated by CL3 prenylation and palmitoylation.

Does CL3 actually share some of the properties known for dendritic raft signaling molecules? A number of raft proteins were previously reported to homo-oligomerize into a multimeric protein complex via lipidification (Zacharias et al., 2002; Huang and El-Husseini, 2005). Indeed, HA-tagged WT CL3 coimmunoprecipitated with GFP-CL3 (Figure 2C) in cortical neurons. Furthermore, a significant fluorescence energy transfer (FRET) was detected between coexpressed CFP-CL3 and YFP-CL3 in live hippocampal neurons, indicative of their genuine molecular proximity in a complex (Figure S2A). Interestingly, Lyn, a well known raft-enriched molecule, colocalized with CL3 in live-untreated, but not in detergent-treated, neurons (Figure S2B). In contrast, the distribution of GluR1, a dendritic protein that is targeted to lipid rafts by palmitoylation (Suzuki et al., 2001; Hering et al. 2003; Hayashi et al. 2005), partially overlapped with CL3 even in detergent-treated neurons (Figure S2C).

CL3 Promotes Dendritogenesis in Cortical Neurons

From previous studies (Takemoto-Kimura et al., 2003; Wayman et al., 2004), it has been speculated that the CaMKK-CaMKI pathway might play a role in the control of neuronal morphology during development. In situ hybridization of embryonic day 17.5 (E17.5) tissues revealed a strong expression of CL3 transcript in the forebrain (Figures 3A and 3B) and in particular in the cortical plate of the cerebral cortex (Figures 3C and 3D). To test whether CL3 was involved in neuronal morphogenesis during this period, either GFP or GFP-CL3 cDNAs were

electroporated into cortical neurons immediately upon dissociation, and the morphology of the neurons was examined 48 hr later, a time point when the majority of neurons under our culture conditions developed well-discernable dendrites and one axon. In control GFP-expressing neurons, little GFP fluorescence overlapped with a Golgi membrane marker, GM130 (Figures 3E and 3F, arrow). In GFP-CL3-overexpressing cortical neurons, however, GFP fluorescence colocalized with GM130 (Figures 3G and 3H, arrow) and also showed discrete enrichment within several dendritic processes (Figures 3G and 3H, arrowhead). Compared to GFP-expressing control neurons (Figure 3I), GFP-CL3-overexpressing neurons appeared to exhibit unaltered axonal extension and branching, while in contrast, increased dendritic growth was found at and in the very vicinity of the soma (Figure 3L). In keeping with this finding, coexpression of mCherry-actin with GFP-CL3 (Figures 3M and 3N), but not with GFP (Figures 3J and 3K), revealed an augmentation of actin-enriched tips at the growing ends (Figures 3M and 3N, arrows) of the nascent processes extending out from the soma, consistent with activation of an actin cytoskeletal remodeling process. To quantify the morphological changes associated with CL3 overexpression, morphometric analyses were performed on the dendrites of GFP-CL3-expressing cortical neurons in a blind fashion. We found that total dendritic length, and in particular the length of the longest dendrite, was most strikingly increased by CL3 overexpression, while the change in branch-tip number remained small and not significant (Figure 3O). CL3-dependent promotion of dendritic growth was detected equally over the whole range of length of primary dendrites (Figure 3P), suggesting that the CL3 effect was unlikely to be restricted to just a subgroup of dendrites, but rather promoted a key common step in early dendritic formation. This CL3-induced effect was not seen with a kinase-inactive K52A mutant (data not shown). Together, these sets of evidence suggested the possibility that CL3 may be involved in early stages of dendritogenesis in developing cortical neurons.

A Required Role of CL3 in Dendritogenesis but Not in Axonogenesis

To critically test this possibility, we next examined the neuronal morphology in neurons where CL3 expression was strongly attenuated by RNA interference, using a short hairpin-type pSUPER vector that also coexpressed a PGK promoter-driven EGFP or mRFP1 gene cassette for morphological tracing. The knockdown efficiency and specificity of the shCL3 vector was prominent enough such that even an overexpressed GFP-CL3 became barely detectable 48 hr after transfection, while the control mRFP1 expression level remained unchanged (Figure 4A). This shCL3 vector was introduced into embryonic cortical neurons by electroporation, and formation of dendrites and axons was studied 48 hr later. While the cortical neurons showed 5–6 dendritic processes in control experiments, shCL3-treated neurons revealed a notable impairment in the number and total length of MAP2-positive dendrites (Figure 4B, arrows). In striking contrast, formation of Tau-1-positive axons was largely spared (Figure 4B, arrowheads). Quantitative morphometric analyses on dendritic or axonal arborizations confirmed that the impairment in shCL3-transfected neurons was actually confined to a selective decline in total dendritic length and in total tip number and did not affect either axonal outgrowth or branching (Figures 4C and 4D). The reduction in dendritic growth was observed throughout the whole range of dendrite length (Figure S3). The striking specificity in dendritic phenotype was also sustained even in shCL3-transfected neurons that were plated following an extensive period (48 hr) of suspension culture that allowed them to maximize the effect of knockdown prior to plating (Figure S4). Knockdown of either CaMKIIα or CaMKIV revealed no phenotype, at least during the very early dendritogenic period that we examined (Figure S5). Taken together, knockdown of CL3 did not interfere with the process of axon specification or axonogenesis, but rather suppressed a subsequent process that was required for dendritogenesis. We next asked whether CL3's kinase activation was a genuine requirement. The abnormality in dendritogenesis could be rescued by additional expression of an shCL3-resistant WT (kinase-active) CL3, but not by that of an shCL3-resistant K52A (kinase-inactive) CL3, demonstrating the absolute necessity of CL3 kinase activity during dendritogenesis (Figure 4E). Consistently, early dendritogenesis, but not axonogenesis, was also impaired in cultured cortical neurons obtained from CL3 null mice (Figure 4F).

In 9 DIV hippocampal neurons, CL3 knockdown diminished total dendritic length and primary dendrite number (Figure S6) and induced an altered Golgi morphology (Figure S7), which was somewhat reminiscent of Golgi vesiculation associated with impaired dendritic polarity (Horton et al., 2005).

A Required Role for CL3 in BDNF-Stimulated Dendritic Growth

We then asked what calcium mobilization might contribute to CL3-dependent stimulation of dendrite development. Brain-derived neurotrophic factor (BDNF) was previously shown to strongly promote dendrite growth and trigger an intracellular calcium rise (e.g., Huang and Reichardt, 2003, for a review). Consistent with published literature, bath application of BDNF induced a slow but clear increase in intracellular Ca^{2+} concentration in the cultured cortical neurons used in our study (Figures 5A–5C). Latencies of onset and oscillatory amplitudes/frequencies varied from neuron to neuron (Figures 5B and 5C). Continuous treatment of cortical neurons with BDNF significantly promoted dendritic growth (Figure 5D, $p < 0.05$, ANOVA with post hoc Tukey-Kramer test). In the presence of a global blocker of CaM kinase activation, KN-93, both constitutive and BDNF-stimulated components of dendritic growth were strongly inhibited

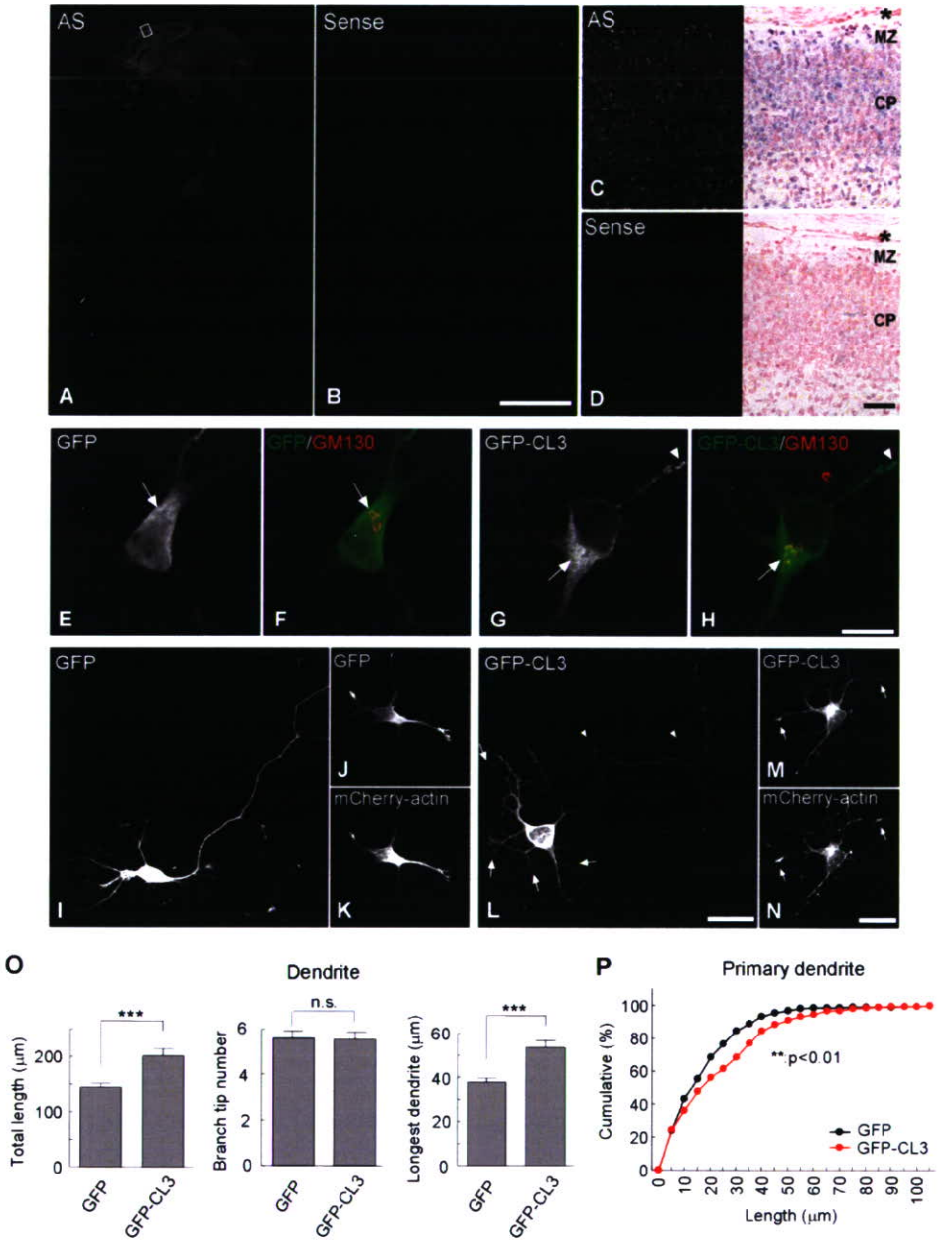

Figure 3. Expression of CL3 in the Developing Cortex and Regulation of Dendritic Morphogenesis in Cultured Cortical Neurons

(A–D) In situ hybridization of mouse embryonic (E17.5) tissue using an antisense (AS) riboprobe revealed an intense signal of CL3 transcript in the developing forebrain. The boxed area of a macroscopic image in (A) is shown at higher magnification (C): (left) hybridized DIG signal only; (right) full-color image (DIG signal in blue-violet + nuclear counterstaining in red). The control sense probe detected little signal (B and D). Asterisk, pia mater; MZ, marginal zone; CP, cortical plate.

(E–H) Membrane localization of CL3 in embryonic cortical cultures. GFP-CL3 distribution detected by anti-GFP immunostaining (G and H) showed colocalization with a Golgi marker, GM130 ([G and H], arrows). GFP-CL3 signals were also enriched within tips of fine dendritic processes ([G and H], arrowheads). Note that the GFP signals in control neurons were separated from the red GM130 immunofluorescence (E and F). Single representative confocal sections are shown.

(I–N) Overexpression of GFP-CL3 facilitated formation of actin-rich thin processes from dendrites and soma. Low-magnification image showed GFP-CL3 signals were distributed both in the nascent dendrites and in the axon ([L], arrow and arrowhead, respectively). In GFP-CL3-expressing neurons, a larger number of thin processes reminiscent of fine dendrites and/or filopodia were present at dendrites and soma ([L and M], arrows), as compared with GFP-expressing neurons (I and J), but not at the axon ([L], arrowheads). These numerous processes contained abundant amounts of β-actin, as shown by enrichment of mCherry-actin (arrows in [N]).

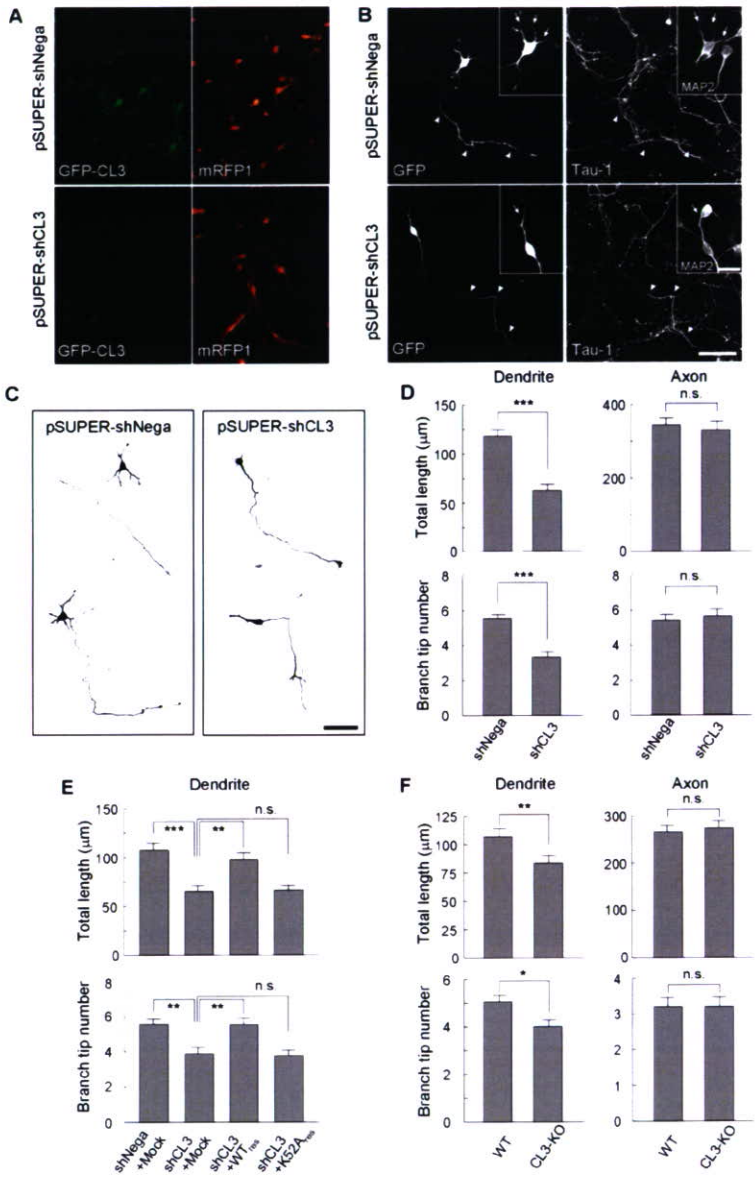

Figure 4. CL3 Loss-of-Function in Embryonic Cortical Neurons Elicits a Specific Impairment in Dendrite Morphogenesis

(A) Efficient downregulation of exogenous GFP-CL3 was achieved by a CL3-targeted shRNA vector (pSUPER-shCL3), but not by a control vector (pSUPER-shNega), in embryonic cortical neurons. The mRFP1 expression, which was driven by a dual promoter in a pSUPER + mRFP1 vector cassette, remained unchanged.

(B) A representative confocal image of an shCL3/GFP-expressing neuron (pSUPER-shCL3) showing impaired dendritogenesis. In this example, an shCL3-expressiong neuron had only a single remaining dendrite (an arrow in the inset), while an shNega-transfected neuron carried 5–6 dendrites (arrows in the inset). On the other hand, no change in axonal morphology was detected (arrowheads). Tau-1 and MAP2 were used to identify axons and dendrites, respectively.

(C) Monochrome diagrams of representative shNega- or shCL3-expressing neurons. The longest process (axon) was unchanged, while the morphology of shorter dendrites near the cell soma was much simplified in shCL3-transfected neurons.

(D) Quantification of morphometric parameters in CL3-knockdown neurons. To quantify, the total length and the dendritic branch tip number were calculated over the dendritic or the axonal arborizations for all branches exceeding 7 μm in length. In shCL3-expressing neurons, both parameters were significantly reduced in the dendrites. On the other hand, neither axonal length nor axonal branch tip number were significantly altered. Number of neurons: shNega, n = 78; shCL3, n = 53. ***$p < 0.001$; n.s., not significant ($p > 0.05$) (t test).

(E) Requirement for CL3 kinase activity to rescue shCL3-mediated impairment in dendritogenesis. Introduction of an shCL3-resistant silent mutant of wild-type GFP-CL3 (WT_{res}) successfully rescued the dendritic phenotype elicited by shCL3 on both morphometric parameters. The shCL3-resistant kinase-inactive GFP-CL3 ($K52A_{res}$) was unable to rescue the shCL3 phenotype. Number of neurons: shNega, n = 37; shCL3 + mock, n = 35; shCL3 + WT_{res}, n = 41; shCL3 + $K52A_{res}$, n = 33. **$p < 0.01$; ***$p < 0.001$; n.s., not significant ($p > 0.05$) (ANOVA with post hoc Tukey-Kramer test).

(F) Dendritogenesis, but not axonogenesis, is specifically impaired in cultured cortical neurons from CL3-KO mice. WT, n = 20; CL3-KO, n = 20. *$p < 0.05$; **$p < 0.01$; n.s., not significant ($p > 0.05$) (t test). Scale bars, 50 μm (A–C) and 20 μm ([B], inset).

(Figure 5D). Because KN-93 suppressed dendritic growth to a similar extent under either constitutive or BDNF-stimulated conditions, this raised the possibility of a common involvement of a KN-93-sensitive kinase (Figure 5D). To specifically test this idea, we employed RNAi and measured the degree of suppression of dendritic growth in the absence or presence of BDNF application and found that indeed CL3 knockdown completely phenocopied the effect of KN-93 on dendrites and occluded BDNF-stimulated dendritic growth (Figure 5E).

(O) Facilitation of dendritic outgrowth by CL3 overexpression. Total length, branch tip number, and longest dendrite length are shown. Number of neurons: GFP, n = 30; GFP-CL3, n = 30. ***$p < 0.001$; n.s., not significant ($p > 0.05$) (t test).

(P) Cumulative probability analysis shows a significant extension of primary dendrites in GFP-CL3-expressing neurons (**$p < 0.01$, Kolmogorov-Smirnov test). Numbers of examined dendrites: GFP, n = 258 (from 50 neurons); GFP-CL3, n = 321 (from 50 neurons).

Scale bars, 300 μm (A and B); 50 μm (C and D); 10 μm (E–H); 20 μm (I–N).

Furthermore, dendritic growth was rescued by coexpressing an shCL3-resistant wild-type, but not a membrane anchoring-defective CL3 mutant (Figure 5F). Thus, signaling via membrane-anchored CL3 may play a critical role in BDNF-mediated cortical dendritogenesis during early development.

A Lipid-Raft-Delineated CL3-STEF-Rac Pathway Contributes to the Development of Cortical Dendrites

What are the signaling components that underlie lipidified CL3-mediated dendritic growth? Taking advantage of our finding that CL3 overexpression was accompanied by a sizable increase in the length of primary dendrites (Figures 3O, 3P, and 6A), and in particular its longest dendrite (Figure 3O, right panel; Figure 6B), we next tested the possible contribution of small GTPases downstream of CL3. Coexpression of a dominant-negative Rac abolished the effect of CL3 overexpression (Figures 6A and 6B), and this effect was seen throughout the observed range of primary dendrite length (Figure 6C), supporting the idea that Rac mediated CL3-stimulated dendritic growth. Consistently, we found that CL3 knockdown downregulated Rac activity (Figure 6D). Furthermore, overexpression of a dominant interfering fragment (PHnTSS) of STEF, a specific RacGEF previously implicated in cortical migration and neurite outgrowth (Kawauchi et al., 2003; Matsuo et al., 2002), also potently repressed the CL3 effect (Figures 6A and 6B); however, this effect was less pronounced in dendrites with shorter lengths (<20 μm) (Figure 6C). Both STEF and Rac were detected in the Triton X-100-insoluble low-density membrane fractions enriched for flotillin-1 but devoid of transferrin receptors (Figure 6E), consistent with the presence of a raft-delineated CL3-STEF-Rac pathway. In keeping with this, sustained Rac activity significantly attenuated the impairment in dendrite development observed in CL3-diminished neurons (Figures 6F and 6G).

If raft localization of CL3 was critical for CL3-dependent dendritogenesis, a raft depletion by pharmacological manipulation or a removal of CL3 from rafts by mutation of its palmitoylation sites should significantly perturb dendrite formation and growth. To test this, we pretreated cortical neurons with either mevastatin, an HMG-CoA reductase inhibitor, to deplete membrane cholesterol, and/or with fumonisin B_1, an inhibitor of sphingolipid synthesis. Treatment with either mevastatin or, to a lesser extent, with fumonisin B_1 reduced dendritogenesis (Figures 7A and 7B). A combination of both had no further additive effect (Figures 7A and 7B). As mevastatin was expected to interfere not only with cholesterol synthesis alone but also with protein prenylation, we also examined the effect of zaragozic acid, an inhibitor of squalene synthase, which would disrupt cholesterol synthesis while sparing mevalonate production. Zaragozic acid treatment diminished dendrite formation to a degree similar to the effect seen with mevastatin; a combination of both did not produce a further incremental effect (Figures 7A and 7B). Interestingly, raft depletion by treatment with zaragozic acid abolished the dendritogenic action of overexpressed CL3 (Figure 7C). Together, these results further supported the idea that the presence of intact lipid rafts was critical for CL3 to exhibit its dendritic effect.

In keeping with this, a palmitoylation-site-deficient 4CS mutant of CL3, which was made resistant to shCL3 RNAi vector, was unable to rescue the dendritic effect of CL3 knockdown in cortical neurons (Figure S4C). Intriguingly, in hippocampal neurons, the inaccessibility of 4CS mutant protein toward detergent-resistant raft membranes in CL3-knockdown cells (Figure S8A) was accompanied with the appearance of exuberant thin filopodial processes from the soma (Figure S8B, arrows). These results are consistent with a role of palmitoylation in targeting, and perhaps restricting, CL3 expression to its appropriate sites of cellular actions. Taken together, CL3 palmitoylation may be a useful means to restrict STEF-Rac activation to microdomains in the vicinity of dendritic rafts during early dendritogenesis.

DISCUSSION

Identification of CL3/CaMKIγ as a Privileged Kinase Involved in the Regulation of Dendritic Cytoarchitecture during Early CNS Development

Previous analyses have established the necessity of CaMKII, a predominant form of CaM kinase, as molecular switch required for neuroplasticity in the hippocampus, the barrel cortex, and the visual cortex (Lisman et al., 2002; Fox and Wong, 2005). Furthermore, the role of CaMKII isoforms in several forms of dendritic development was extensively studied, though the exact effect on dendrite morphogenesis has remained rather controversial. CaMKIIα was shown to contribute to dendritic outgrowth in cerebellar granule neurons (Gaudilliere et al., 2004), and CaMKIIβ but not CaMKIIα regulated the movement and branching of filopodia and fine dendrites in rat hippocampal neurons (Fink et al., 2003). In contrast, in *Xenopus* retinotectal neurons, CaMKII was reported to limit dendritic outgrowth and to stabilize dendritic arborization in vivo (Wu and Cline, 1998).

In contrast to CaMKII, which is one of most abundant proteins expressed in the postsynaptic density (PSD) (Kennedy, 2000), CaMKIV in the nucleus plays a critical role in mediating Ca^{2+}-regulated transcription via a CREB/CBP pathway, which is necessary for the formation of long-term synaptic plasticity and long-term memory (Silva et al., 1998; Bito and Takemoto-Kimura, 2003), as well as activity-dependent dendritic elongation (Redmond et al., 2002). In turn, a cytosolic CaMKI activity has been shown to participate in the gating of an ERK/MAP-kinase-dependent form of LTP (Schmitt et al., 2005). Neurite outgrowth was also reported to be regulated by a presumably cytosolic CaMKK-CaMKI/IV pathway: indeed, a constitutively active CaMKIV was suggested to enhance dendritic growth via stabilization of β-catenin (Yu and Malenka, 2003), while a CaMKK inhibitory drug, STO-609, or putative dominant-negative constructs specifically blocking

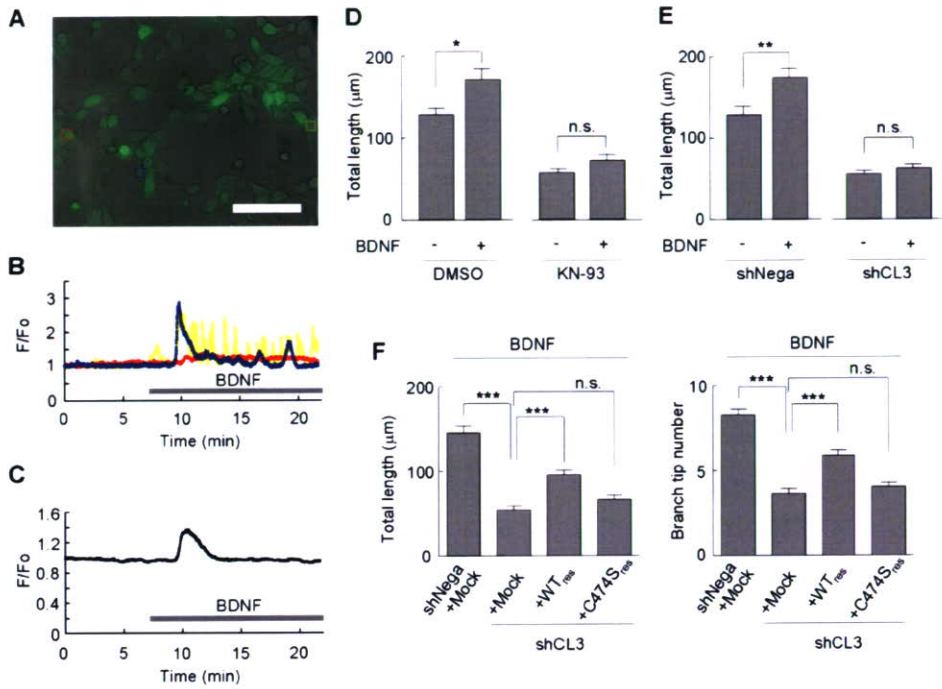

Figure 5. Requirement of CL3 for BDNF-Stimulated Dendrititogenesis

(A) BDNF-induced calcium transients in developing cultured neurons. A representative image of cortical neurons during a typical calcium rise after BDNF bath application is shown in (A). Embryonic cortical neurons (1 DIV) were loaded with a calcium indicator, Fluo-4AM, and calcium responses were measured by time-lapse imaging. A green fluorescence image was overlaid on a DIC image. Colored boxes indicate the location of cells shown in (B). Scale bar, 50 μm.

(B) Representative calcium responses in individual cells after BDNF administration. Three different types of calcium responses were revealed. The majority of cells showed a large transient response followed by smaller repetitive responses (blue), whereas some showed oscillation (yellow) or chronic increases from the baseline (red).

(C) Averaged calcium responses after BDNF administration. An averaged response from 70 cells in a microscopic field is shown.

(D) Cortical neurons were transfected with a morphological tracer, mCherry, and stimulated with BDNF from 6 hr to 48 hr after plating, in the presence or absence of KN-93, a general CaM kinase inhibitor. BDNF treatment maximized dendritogenesis, and this BDNF-stimulated increment was occluded in neurons treated with KN-93. Numbers of neurons: vehicle + DMSO, n = 25; vehicle + KN-93, n = 44; BDNF + DMSO, n = 38; BDNF + KN-93, n = 32.

(E) Quantification of dendritogenesis in BDNF-stimulated CL3-knockdown neurons. CL3 knockdown severely inhibited dendritogenesis induced by BDNF administration, to an extent similar to that obtained with KN-93. Numbers of neurons: vehicle + shNega, n = 40; vehicle + shCL3, n = 41; BDNF + shNega, n = 40; BDNF + shCL3, n = 40.

(F) Suppression by CL3 knockdown of BDNF-stimulated dendritogenesis can be rescued by coexpression of an shRNA-resistant wild-type CL3 (WTres), but not by a nonlipidified mutant CL3 (C474Sres). Numbers of neurons: shNega + mock, n = 52; shCL3 + mock, n = 57; shCL3 + WTres, n = 57; shCL3 + C474Sres, n = 55.

***p < 0.001; n.s., not significant (ANOVA with post hoc Tukey-Kramer test).

either CaMKK or cytosolic CaMKI/CaMKIV (but not nuclear CaMKIV) activities prevented axonal extension and growth cone dynamics as well as neurite extension (Schmitt et al., 2004; Wayman et al., 2004).

Taken together, multiple CaM kinase pathways that are segregated in distinct subcellular compartments may regulate several critical steps converging onto dendrite elongation and maturation. This prompted us to investigate the particular role of CL3/CaMKIγ (Takemoto-Kimura et al., 2003; Nishimura et al., 2003), a membrane-anchored form of CaMKI, which was highly expressed in the cortical plate neurons of the mouse embryo (this study). Intriguingly, we found a specific impairment in the number and total lengths of dendrites in CL3 knockdown and CL3 null neurons (Figure 4 and Figure S3), while axonal morphology was not significantly distinct from controls. Knockdown of CL3 prior to plating of neurons strengthened this suppressive effect on the dendrites while still sparing the axons (Figure S4). Taken together, our data suggested a prominent role of CL3 during the early stages of dendritogenesis that presumably followed completion of the axon/dendrite specification.

While this paper was under review, an independent study reported that CL3/CaMKIγ may regulate activity-dependent dendritic growth at an even later stage of development in hippocampal neurons (Wayman et al., 2006; see also Figures S6 and S7 of this study).

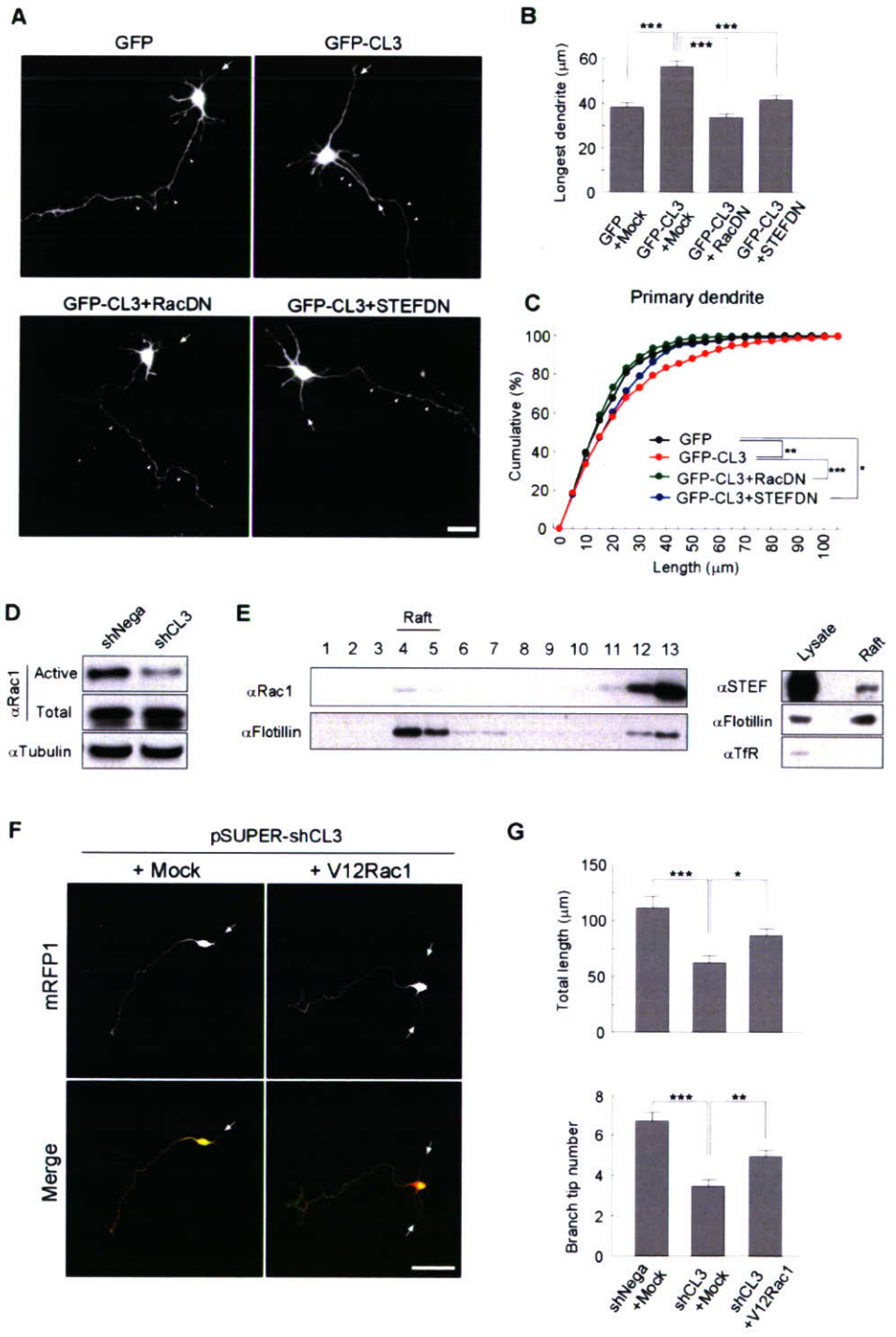

Figure 6. A Critical Role for RacGEF STEF and Rac in Mediating CL3-Induced Dendritic Outgrowth

(A) Cortical neurons were cotransfected with GFP-CL3 and either dominant-negative Rac1 (RacDN) or dominant-interfering fragment of STEF (STEFDN) together with a morphometric tracer, mRFP1. Examples for dendrites (arrows) and axons (arrowheads) are shown. Scale bar, 20 μm.

(B) Quantification of longest dendrite. Number of neurons: GFP + mock, n = 51; GFP-CL3 + mock, n = 50; GFP-CL3 + RacDN, n = 57; GFP-CL3 + STEFDN, n = 60. ***p < 0.001 (ANOVA with post hoc Tukey-Kramer test).

(C) Cumulative probability analysis of the length of primary dendrites showed that inhibition of STEF and Rac activity suppressed the extension of primary dendrites induced in GFP-CL3-expressing neurons. Number of examined dendrites (neurons): GFP, n = 324 (from 51 neurons); GFP-CL3, n = 332 (from 50 neurons); GFP-CL3 + RacDN, n = 328 (from 57 neurons); GFP-CL3 + STEFDN, n = 378 (from 60 neurons). *p < 0.05; **p < 0.01; ***p < 0.001 (Kolmogorov-Smirnov test).

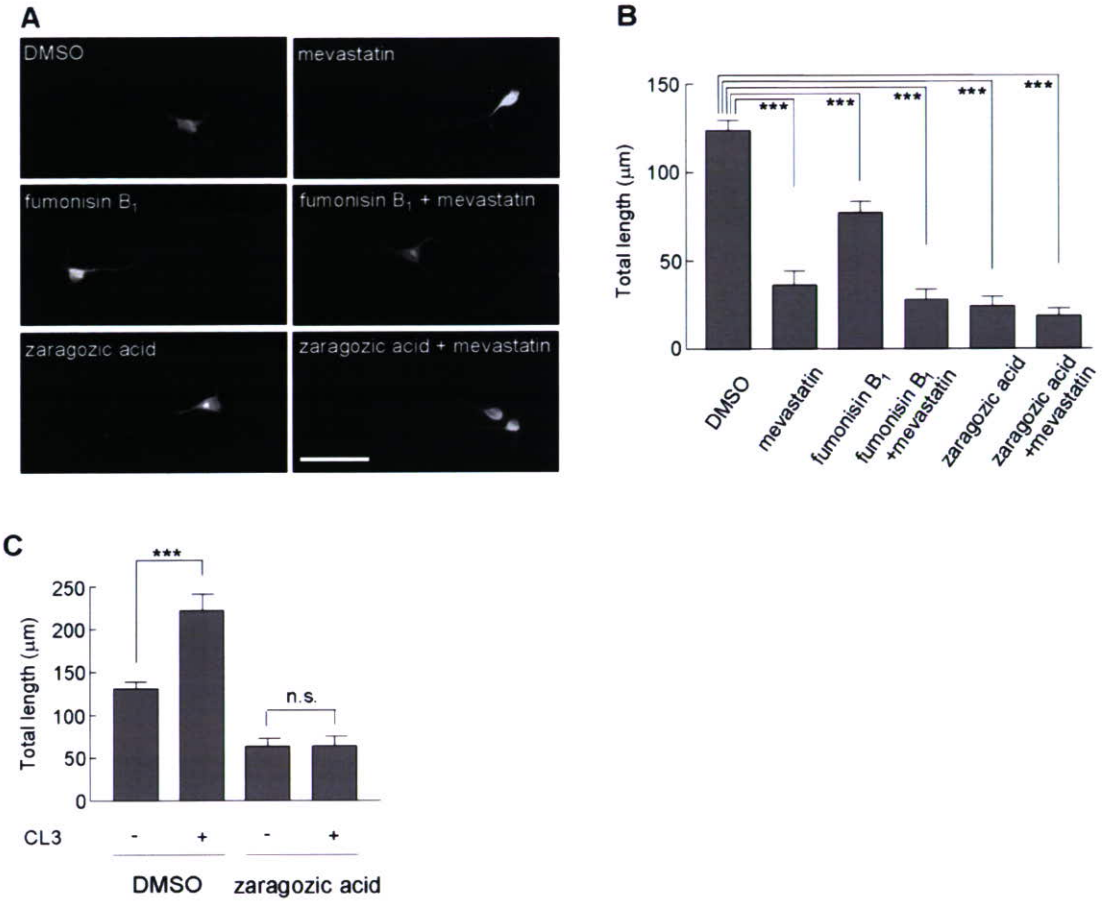

Figure 7. Raft Depletion Abolishes CL3-Mediated Dendrite Outgrowth

(A) Cortical neurons were transfected with a morphological tracer, mCherry, and cultured in the presence of various combinations of raft-depleting agents from 6 hr to 48 hr after plating. Disruption of cholesterol/sphingolipid synthesis strongly inhibited formation and outgrowth of the dendritic processes around the soma. Scale bar, 50 μm.

(B) Ensemble average of experiments shown in (A). DMSO, n = 10; 10 μM mevastatin, n = 15; 10 μM fumonisin B_1, n = 15; 10 μM fumonisin B_1 and 10 μM mevastatin, n = 15; 100 μM zaragozic acid, n = 15; 100 μM zaragozic acid and 10 μM mevastatin, n = 15. ***$p < 0.001$ (ANOVA with post hoc Tukey-Kramer test).

(C) Raft depletion using zaragozic acid abolished the increase of dendritogenesis induced by CL3 overexpression. A significant CL3-mediated increase in dendritic growth was shown in the DMSO control, but this significant increase was abolished by raft depletion in the presence of zaragozic acid (two-way ANOVA, CL3 effect, $F_{1,65} = 8.65$, $p = 0.0045$; drug effect, $F_{1,65} = 51.95$, $p < 0.0001$; CL3 × drug, $F_{1,65} = 8.38$, $p = 0.0052$). ***$p < 0.001$ (post hoc Bonferroni test). DMSO, n = 15 (−CL3), n = 24 (+CL3), 100 μM zaragozic acid, n = 15 (−CL3), n = 15 (+CL3).

Control of CL3 Targeting to Lipid Microdomains by a Kinase-Activity-Regulated Dual Lipidification Mechanism

In polarized neural cells, covalently attached lipid modification of proteins is important for membrane targeting and expression of proper function in the vicinity of specialized membrane compartments. Largely based on quantitative work on Ras and PSD-95, a palmitoylation/depalmitoylation cycle has been previously suggested to play a crucial regulatory role in determining the proper

(D) The amount of GTP-bound active Rac1 was measured by a Pak1-PBD pulldown assay using cortical neurons transfected with shNega or shCL3 vector. The amount of active Rac1 was reduced by CL3 knockdown.

(E) Presence of Rac1 and STEF immunoreactivities in lipid raft fractions of cortical neurons. For STEF detection, a pooled and concentrated raft fraction was used. Transferrin receptor was used as a non-raft membrane marker.

(F) Representative images of shCL3/mRFP1-expressing neurons coexpressing constitutively active GFP-Rac1 (+V12Rac1) or GFP (+mock). Expression of constitutively-active GFP-Rac1 (+V12Rac1) restored appearance of multiple dendrites (arrows) in shCL3-expressing neurons, while expression of GFP alone did not. Scale bar, 50 μm.

(G) Quantification of dendritic morphogenesis confirmed that constitutively active GFP-Rac1 attenuated the specific impairment of dendritic morphology induced by shCL3 transfection. Number of neurons: shNega + mock, n = 22; shCL3 + mock, n = 47; shCL3 + V12Rac1, n = 49. *$p < 0.05$; **$p < 0.01$; ***$p < 0.001$ (ANOVA with post hoc Tukey-Kramer test).

trafficking and function of palmitoylated signaling proteins (Huang and El-Husseini, 2005). Dynamic regulation of palmitoylation was already shown for a large number of synaptic constituents such as AMPA-receptor subunits (Hayashi et al., 2005), GABAR γ-subunits (Keller et al., 2004), and GRIP/ABP (DeSouza et al., 2002), indicating a critical role for neuronal PAT in synaptic maturation and maintenance. However, a direct involvement of protein palmitoylation in early stages of neuronal morphogenesis has not been examined.

In this work, we demonstrated that the C-terminal end of CL3 was covalently modified in a sequential manner by prenylation and by palmitoylation. A dually lipidified CL3 was generated in a kinase-activity-dependent manner, in part via the PAT GODZ (Uemura et al., 2002), resulting in an efficient enrichment into dendritic-raft-like lipid microdomains.

We then found that dually lipidified CL3 was likely to be partitioned and targeted to close proximity of dendritic lipid microdomains. Consistently, CL3 showed self-association (Figure 2C and Figure S2A), a property that is not unusual for palmitoylated or dually lipidified proteins (Zacharias et al., 2002). However, we failed to detect any Ca^{2+}/CaM-independent kinase activity of CL3, even under conditions where CL3 multimerization was present. This is distinct from the property of CaMKII, in which dodecamerization was shown to promote a Ca^{2+}/CaM-independent kinase activity that outlasted the duration of the incoming Ca^{2+} mobilization through an autophosphorylation mechanism. We thus speculate that oligomerization, if any, of prenyl-/palmitoyl-CL3 may have roles other than the generation of an autonomous kinase activity, such as sustaining a high degree of molecular proximity and concentration that favors signal amplification and increases the specificity and efficiency of coupling to downstream signaling events.

A BDNF-CL3-Rac Pathway May Underlie Excitation-Morphogenesis Coupling during Early Cortical Dendritogenesis

Previously, neuronal activity has been shown to promote initiation of dendrite formation via small GTPases such as Rac and Cdc42 (Luo, 2002; Van Aelst and Cline, 2004). To date, however, knowledge about how neuronal activity regulates these small GTPases is still limited. The strongest evidence in favor of activity-induced dendritic arborization so far involved several Ca^{2+}-regulated transcriptional factor such as CREB, NeuroD, and CREST (Gaudilliere et al., 2004; Konur and Ghosh, 2005), though the cellular mechanisms linking nuclear events and neuronal morphogenesis remained as yet largely undetermined. Here we found that a membrane-bound CaM kinase, CL3/CaMKIγ, may possibly act downstream of BDNF and Ca^{2+} signals to promote dendritic cytoskeletal remodeling via the small GTPase Rac, especially during early stages of dendritic development. Furthermore, we provided several lines of evidence that collectively indicated that CL3-STEF-Rac signaling triggered at or in the vicinity of lipid rafts may play a critical role.

Could lipid rafts, also known as sphingolipid- and cholesterol-rich membrane microdomains, be distributed in an asymmetric fashion such that some of these may influence dendrite targeting of signaling proteins such as CL3? In support for such an idea, depletion of cellular cholesterol/sphingolipid content in cultured neurons revealed an important role for cholesterol (Fan et al., 2002) or sphingolipids (Schwarz and Futerman, 1998; Pelled et al., 2003) in dendritic growth and spine maintenance (Hering et al., 2003). In addition, no responsiveness to glutamate application was reported in neonatal cortical neurons of a mutant mouse deficient in cholesterol biosynthesis, despite a normal amount of GluR and NMDAR subunit expression, indicating a possible defect in membrane insertion of dendritic glutamate receptors (Wassif et al., 2001). A distinct kind of raft-mediated asymmetry may play a role in axonal fate specification (Da Silva et al., 2005).

If raft formation was coupled with the creation of a polarized asymmetry of signaling molecule distribution, how could this possibly underlie a morphogenetic response, especially downstream of BDNF? Recruitment of activated TrkB to lipid rafts (Suzuki et al., 2004) could evidently contribute to efficient coupling to raft-targeted CL3 downstream of BDNF. In neurons, fractionation experiments during development have also previously revealed a privileged association of Rac with rafts, but not of RhoA or Cdc42 (Kumanogoh et al., 2001; see also Figure 6E). We additionally found that a portion of STEF was clearly present in the raft fractions as well (Figure 6E). As the fragment encompassing the PHnTSS domain of STEF (PHnTSS) has been shown to act as a specific dominant-negative form for both STEF and Tiam1 (Matsuo et al., 2002), it remains possible that there may also be an additional contribution of Tiam1, a known substrate for CaMK activity (Tolias et al., 2005).

Taken together, dual lipidification of CL3 may be an efficient mechanism not only to target it into rafts and to limit its protein diffusion parallel to the lipid bilayer, but also to generate a membrane-delimited area of Rac activation within segregated dendritic lipid microdomains at the vicinity of Ca^{2+}-mobilization events. Further studies are needed to substantiate such a hypothesis.

In conclusion, we here uncovered a novel role for CL3/CaMKIγ in the regulation of Rac-dependent dendritic cytoskeletal reorganization, and we found evidence for CL3 in mediating BDNF-stimulated dendritic growth. Through a dual and sequential lipidification mechanism, the unique C-terminal region of CL3 was covalently lipid-modified in a kinase-activity-dependent manner, leading to a privileged partition of membrane-anchored CL3 into dendritic-raft-like lipid microdomains. This membrane-sorting mechanism, unprecedented for a neuronal Ser/Thr kinase, in turn may efficiently localize Rac activity and thereby regulate dendritogenesis. Thus, CL3 turned

out to represent a key element in the Ca^{2+}-dependent and lipid-raft-delineated switch that turned on activity-regulated dendrite formation in developing cortical neurons.

EXPERIMENTAL PROCEDURES

Cloning and Plasmid Constructions

A detailed description of all plasmids can be found in the Supplemental Data.

Immunocytochemistry

Cells were fixed in 4% paraformaldehyde/4% sucrose/phosphate-buffered saline (PBS) (−) at room temperature for 20 min, and immunostaining was carried out as described (Takemoto-Kimura et al., 2003). Additional methods can be found in the Supplemental Data.

Western Blot Analysis

For western blot analysis, primary antibodies were as follows: rat anti-GFP (Nacalai Tesque, Japan), rat anti-HA (Roche Diagnostics), mouse anti-Flotillin-1, mouse anti-Caveolin-2, and anti-Rac1 (BD Transduction Laboratories). A rabbit anti-STEF antibody was as described (Matsuo et al., 2002). Chemiluminescence detection was performed using HRP-conjugated anti-rat and anti-mouse IgG and ECL-Plus reagent (Amersham Biosciences).

Metabolic Labeling and Coimmunoprecipitation

For metabolic labeling, COS-7 cells plated onto 6-well plates were transfected with wild-type and mutant GFP-CL3 vectors using Fugene6 reagent (Roche Diagnostics). For mevalonate labeling, a pMev vector (ATCC), which encoded a transporter that augmented mevalonic acid uptake, was cotransfected with GFP-CL3 for 24 hr. Cells were pretreated with 40 μM Compactin (Wako, Japan) for 2 hr, then incubated for 20 hr in growth medium supplemented with 40 μM Compactin and 0.1 mCi/ml of [^{3}H]-mevalonolactone (PerkinElmer or ARC). Palmitate labeling was initiated 48 hr after transfection by pretreating cells with serum-free medium (DMEM with 1% fatty-acid-free bovine serum albumin [Sigma]) for 1 hr, and then incubating for an additional 3 hr in the serum-free medium supplemented with 0.4 mCi/ml of [^{3}H]-palmitic acid (PerkinElmer). After metabolic labeling, cells were washed twice in ice-cold phosphate-buffered saline (PBS) (−) and lysed in lysis buffer containing 50 mM Tris-HCl (pH 7.5), 100 mM NaCl, 2 mM $MgCl_2$, 10% glycerol, 1% Triton X-100, and a Complete protease inhibitor cocktail (Roche Diagnostics). Lysates were immunoprecipitated using a rabbit anti-GFP polyclonal antibody (Molecular Probes) and Protein-A-Sepharose (Amersham Biosciences). Immunoprecipitates were washed three times in lysis buffer and boiled in 4× Laemmli buffer containing 5 mM DTT for 3 min and were subjected to SDS-PAGE. Incorporated mevalonolactone and palmitic acid were digitally detected using a BAS-5000 bioimage analyzer and quantified using Multi Gauge software (Fujifilm, Japan).

In coimmunoprecipitation assays, cortical neurons were transfected with GFP-CL3 and HA-CL3 vectors by electroporation using Nucleofector (Amaxa Biosystems) and plated onto poly-D-Lysine-coated 6 cm dishes at the density of 4 × 10^5/cm^2 and then harvested at 2 DIV. Immunoprecipitation was performed as described above.

Lentivirus Production, Infection, and Lipid Raft Fractionation

A 536 bp synapsin I promoter was isolated by PCR from rat genomic DNA and inserted into CS-CA-MCS (Miyoshi et al., 1998) to replace the original chicken actin promoter. EGFP-CL3 fragment was further inserted and cotransfected with pCAG-HIVgp and pCMV-VSV-G-RSV-Rev into HEK293T cells using Fugene6 reagent to generate a self-inactivating lentivirus vector. All original lentivirus vectors were provided by Dr. Hiroyuki Miyoshi (RIKEN-BRC, Japan). Concentrated virus solutions were obtained by ultracentrifugation at 80,000 × g, and virus titer was determined using HeLa cells. Cortical neurons (1 DIV) were infected with lentivirus for 5 hr at a nominal MOI of about 0.2, and after washout, maintained in Neurobasal containing 0.5 mM Glutamax, 1 × B27, and 25 μg/ml insulin. Under these conditions, GFP-positive glial cells (as determined by GFAP expression) were less than 6%. Though the nominal MOI was about 0.2, this is very likely to be an underestimate, as it was calculated based on the induction of trace EGFP fluorescence in heterologous cells. Lipid raft preparations were performed 2 days after infection (3 DIV).

Lentivirus-infected cortical neurons in 10 cm dishes (3.5 × 10^5 cells/cm^2) were harvested at 3 DIV for preparation of detergent-insoluble membrane fractions according to Suzuki et al. (2004) with minor modifications. Thirteen fractions (1 ml each) were collected and 15 μl of each fraction were subjected to SDS-PAGE followed by western blot analysis. To obtain a concentrate of the raft fractions in Figure 5E, raft fractions (fractions 4 and 5) were pooled, and a portion of it (1.4 ml) was ultracentrifuged at 20,000 × g for 1 hr at 4°C. The pellet was resuspended in 140 μl of Buffer A (50 mM Tris-HCl [pH 7.5], 50 mM NaCl), and 15 μl of the final sample was subjected to SDS-PAGE and western blot analysis.

Cell Culture Preparation and Visualization of Raft-Targeted Proteins

COS-7 cells were maintained in Dulbecco's modified Eagle medium (DMEM) containing 10% heat-inactivated fetal calf serum (FCS). Dissociated cortical cultures from embryonic day 19 Sprague-Dawley rats were prepared as described previously for rat hippocampal cultures (Bito et al., 1996) with minor modifications. Cortical neurons were plated onto 12 mm poly-L-Lysine-coated coverslips at the density of 5 × 10^5 cells per coverslip in a 24-well plate.

Gene targeting of CL3/CaMKIγ was carried out in a C57BL/6-derived ES cell line RENKA (Mishina and Sakimura, 2007) by insertional mutagenesis. The exons 2 and 3 of mouse the *Camk1g* gene, which contained the kinase ATP-binding site, were deleted and replaced by a targeting construst such that the first methionine of CL3 was fused in-frame to an hCrePR-IRES-EGFP cassette that was juxtaposed to an inverted neomycin resistance gene flanked by FRT sites. A detailed analysis of the CL3/CaMKIγ null mouse mutant will be described elsewhere (S.T.-K., M.O., T. Takeuchi, K. Sakimura, M.M., H.O., and H.B, unpublished data). Cortical mouse cultures were prepared from embryonic day 17 C57BL/6J wild-type or CL3 null mice.

For visualization of in situ raft-targeted GFP-fusion proteins, rat cortical or mouse hippocampal neurons were washed with KRH buffer (Suzuki et al., 2004) containing 2 mM Ca^{2+} on ice, permeabilized with 0.1% Triton X-100/KRH(+) for 2 min on ice, washed gently, and then fixed. Raft depletion in cortical neurons was carried out by including one of the following drugs (10 μM mevastatin, 10 μM fumonisin B_1, 10 μM fumonisin B_1 and 10 μM mevastatin, 100 μM zaragozic acid, 100 μM zaragozic acid, and 10 μM mevastatin) in the culture medium from 6 hr after plating onward for an additional 42 hr. mRFP1 was nucleofected for accurate visualization of the contours of individual neurons.

In one instance, rat hippocampal neurons obtained from P0–1 Sprague-Dawley rats (Bito et al., 1996) were used to quantify FRET between CL3 molecules (Figure S2A).

Morphometric Analysis of the CL3-Associated Phenotype in Cultured Neurons

Dissociated cortical cultures from embryonic day 19 Sprague-Dawley rats were prepared as described previously for rat or mouse hippocampal cultures (Bito et al., 1996; Furuyashiki et al. 2002) with minor modifications. Cortical neurons were transfected immediately after dissociation by electroporation using Nucleofector and plated onto 12 mm poly-L-Lysine-coated coverslips at the density of 5 × 10^5 cells per coverslip (rats) or 7.5 × 10^5 cells per coverslip (mice) in 24-well plates, and then fixed at 2 DIV. Presumably because of a relatively low amount of plasmid transfer across neuronal membranes during electroporation procedure, use of a strong CAG promoter-driven expression cassette was needed to reliably express foreign genes.

Further, to unequivocally ascertain the phenotypes of neurons expressing various shRNA vectors and rescue constructs, we carried out all quantitative analyses based upon immunostaining of the morphometric markers, either GFP or mRFP1 (a kind gift from Dr. Roger Y. Tsien, HHMI, UCSD). This allowed us to obtain clearer images of neuronal contours, thus facilitating morphometric analyses. The transfection efficiency was relatively high (about 50% in our hands using this protocol) when examined within a day after electroporation. Thus, we were able to improve the accuracy of visualization in all morphometric experiments by simply mixing the transfected cells with nontransfected cells prepared in parallel, at a ratio of 1:20 (rats) or 1:10 (mice), before plating. Dendritic and axonal arborizations of most transfected neurons could then be traced in total isolation while they still formed a dense network with neighboring untransfected neurons. Neurons expressing pSUPER-type vectors revealed negligible amounts of either cell death (0%–0.5%) as measured by TUNEL staining (Roche Diagnostics) or dsRNA-induced interferon-like response monitored using a muMx2 promoter-luc vector (a kind gift from Dr. Atsushi Asano, Hokkaido University) (Alvarez et al., 2006).

In the Rac1-rescue experiments, even an intermediate-level expression of a constitutively active Rac mutant, GFP-V12Rac1, using a CAG promoter usually resulted in an aberrant neuronal morphology, such as exuberant lamellipodia formation at the cell soma and premature detachment from the glass coverslip. To circumvent this problem, GFP-V12Rac1 was introduced using a CMV promoter-based plasmid vector, as the observed expression level was lower than that obtained using a CAG promoter vector. A few neurons still showed an aberrant somata size and shape and thus were excluded from analyses.

Images of neuronal morphologies were captured based on immunoreactivities against GFP or mRFP1, using the Olympus BX51 microscopy system with the 20× objective or 40× objective in the cases of CL3-overexpression experiments to visualize fine protrusions for cumulative probability analysis. Dendrites and axons were identified by standard morphological criteria. As the majority of neurons, in our cortical culture preparation, possessed only one clearly classifiable axon and one or more dendrites, neurons with nonpyramidal morphological features (such as multiple axons or no classifiable processes) were excluded from analyses. The total length and the dendritic branch tip number were determined manually using NeuronJ 1.1.0 (Meijering et al., 2004), plug-in software for ImageJ (NIH). Representative images were acquired using the LSM 510META confocal microscope with the 40× objective. All analyses were performed by an observer blinded to the identity of the transfected constructs.

In experiments described in Figure S4, electroporated neurons were initially cultured as a suspension in a growth medium, without plating, in plastic centrifuge tubes at the density of 2×10^6 cells/ml, while neurons were allowed to form aggregation. Forty-eight hours later, aggregated neurons were then dissociated mechanically by gentle pipetting and plated onto 12 mm poly-L-Lysine-coated coverslips at the density of 1×10^5 cells per coverslip. Fixation and analysis were carried out 24 hr later.

Mouse hippocampal neurons were transfected using Lipofectamine 2000 (Invitrogen) at 7 DIV and analyzed at 9 DIV. Morphometric analyses of hippocampal neurons were performed as essentially described above for cortical neurons. Only primary dendrites were traced using ImageJ/NeuronJ software.

In Situ Hybridization

In situ hybridization using DIG technology (Roche Diagnostics) was performed essentially as described (Ohmae et al., 2006). For the generation of antisense and sense cRNA probes, a 374 bp fragment corresponding to the nucleotide position 964–1337 of CL3 was subcloned into pBluescriptII KS+ vector (Stratagene).

BDNF Application and Calcium Imaging in Cortical Neurons

BDNF (generously provided by Dainippon Sumitomo Pharma, Osaka, Japan, by courtesy of Dr. Chikao Nakayama) and/or KN-93 (Calbiochem) were added to cells at 6 hr after plating at the final concentration of 50 ng/ml and 10 μM, respectively. Bath application was performed by dissolving the reagents in one-half volume of the conditioned culture medium and by mixing this gently with the remaining half of the original medium in the dish. No medium change was done thereafter till fixation.

Fluorescent calcium imaging was performed essentially as described previously (Furuyashiki et al., 2002). A detailed description of further experimental conditions can be found in the Supplemental Data.

Rac1 Pull-Down Assays, Measurement of Fluorescence Resonance Energy Transfer, and Quantification of Golgi Deformation

A detailed description of experimental procedures can be found in the Supplemental Data.

Statistical Analysis

Statistical analyses were performed using Prism 4.0 (GraphPad Software) and JMP5.1.2 (SAS Institute). Student's t test was used for comparisons of two groups. One- or two-way analysis of variance (ANOVA) with post hoc Tukey-Kramer or Bonferroni test was used for factorial analysis between more than three groups. The Kolmogorov-Smirnov test was applied to verify whether the bidirectional effect of CL3 manipulation occurred throughout all dendrites or was restricted to a subpopulation. All data are shown as mean ± standard error of means (SEM), unless otherwise mentioned.

Supplemental Data

The Supplemental Data for this article can be found online at http://www.neuron.org/cgi/content/full/54/5/755/DC1/.

ACKNOWLEDGMENTS

We thank A. Asano, Z. Honda, Y. Ihara, A. Miyawaki, H. Miyoshi, S. Narumiya, F. Oyama, B. Sabatini, and R.Y. Tsien for providing plasmids; S. Wada, M. Morishima-Kawashima, and Y. Ihara for a raft fractionation protocol; T. Furuyashiki for generating EGFP-GluR1; K. Ohkubo for assistance with in situ hybridization; and all members of the Bito laboratory for discussion. We acknowledge the invaluable support of H. Mori in designing a successful targeting vector and of T. Takeuchi and K. Sakimura for an ongoing collaboration to generate and characterize CL3 null mice. We are also indebted to assistance from K. Saiki, Y. Kondo, and T. Kinbara. This work was supported in part by Grants-in-Aid from the MEXT and MHLW of Japan, by a JST-SORST investigatorship, and by awards from the Astellas Foundation for Research on Metabolic Disorders, the Brain Science Foundation, the Cell Science Research Foundation, the Japan Foundation for Applied Enzymology, the Kowa Life Science Foundation, the Novartis Foundation (Japan) for the Promotion of Science, the Shimadzu Science Foundation, the Takeda Foundation, the Toray Science Foundation, and the Human Frontier Science Program. N.A.-I. and H.F. are predoctoral fellows, and M.N. is a postdoctoral fellow from the Japan Society for the Promotion of Science.

Received: May 23, 2006
Revised: December 30, 2006
Accepted: May 16, 2007
Published: June 6, 2007

REFERENCES

Alvarez, V.A., Ridenour, D.A., and Sabatini, B.L. (2006). Retraction of synapses and dendritic spines induced by off-target effects of RNA interference. J. Neurosci. *26*, 7820–7825.

Anderson, R.G.W., and Jacobson, K. (2002). A role for lipid shells in targeting proteins to caveolae, rafts, and other lipid domains. Science *296*, 1821–1825.

Bito, H., and Takemoto-Kimura, S. (2003). Ca^{2+}/CREB/CBP-dependent gene regulation: a shared mechanism critical in long-term synaptic plasticity and neuronal survival. Cell Calcium *34*, 425–430.

Bito, H., Deisseroth, K., and Tsien, R.W. (1996). CREB phosphorylation and dephosphorylation: a Ca^{2+}- and stimulus duration-dependent switch for hippocampal gene expression. Cell *87*, 1203–1214.

Ciani, L., and Salinas, P.C. (2005). WNTs in the vertebrate nervous system: from patterning to neuronal connectivity. Nat. Rev. Neurosci. *6*, 351–362.

Cline, H.T. (2001). Dendritic arbor development and synaptogenesis. Curr. Opin. Neurobiol. *11*, 118–126.

Da Silva, J.S., Hasegawa, T., Miyagi, T., Dotti, C.G., and Abad-Rodriguez, J. (2005). Asymmetric membrane ganglioside sialidase activity specifies axonal fate. Nat. Neurosci. *8*, 606–615.

DeSouza, S., Fu, J., States, B.A., and Ziff, E.B. (2002). Differential palmitoylation directs the AMPA receptor-binding protein ABP to spines or to intracellular clusters. J. Neurosci. *22*, 3493–3503.

El-Husseini, A.E.-D., and Bredt, D.S. (2002). Protein palmitoylation: a regulator of neuronal development and function. Nat. Rev. Neurosci. *3*, 791–802.

Fan, Q.W., Yu, W., Gong, J.S., Zou, K., Sawamura, N., Senda, T., Yanagisawa, K., and Michikawa, M. (2002). Cholesterol-dependent modulation of dendrite outgrowth and microtubule stability in cultured neurons. J. Neurochem. *80*, 178–190.

Fink, C.C., Bayer, K.-U., Myers, J.W., Ferrell, J.J.E., Schulman, H., and Meyer, T. (2003). Selective regulation of neurite extension and synapse formation by the β- but not the α-isoform of CaMKII. Neuron *39*, 283–297.

Fox, K., and Wong, R.O. (2005). A comparison of experience-dependent plasticity in the visual and somatosensory systems. Neuron *48*, 465–477.

Fukata, M., Fukata, Y., Adesnik, H., Nicoll, R.A., and Bredt, D.S. (2004). Identification of PSD-95 palmitoylating enzymes. Neuron *44*, 987–996.

Furuyashiki, T., Arakawa, Y., Takemoto-Kimura, S., Bito, H., and Narumiya, S. (2002). Multiple spatiotemporal modes of actin reorganization by NMDA receptors and voltage-gated Ca^{2+} channels. Proc. Natl. Acad. Sci. USA *99*, 14458–14463.

Gaudilliere, B., Konishi, Y., de la Iglesia, N., Yao, G., and Bonni, A. (2004). A CaMKII-NeuroD signaling pathway specifies dendritic morphogenesis. Neuron *41*, 229–241.

Hayashi, T., Rumbaugh, G., and Huganir, R.L. (2005). Differential regulation of AMPA receptor subunit trafficking by palmitoylation of two distinct sites. Neuron *47*, 709–723.

Hering, H., Lin, C.C., and Sheng, M. (2003). Lipid rafts in the maintenance of synapses, dendritic spines, and surface AMPA receptor stability. J. Neurosci. *23*, 3262–3271.

Higgins, D., Burack, M., Lein, P., and Banker, G. (1997). Mechanisms of neuronal polarity. Curr. Opin. Neurobiol. *7*, 599–604.

Hook, S.S., and Means, A.R. (2001). Ca^{2+}/CaM-dependent kinases: from activation to function. Annu. Rev. Pharmacol. Toxicol. *41*, 471–505.

Horton, A.C., Racz, B., Monson, E.E., Lin, A.L., Weinberg, R.J., and Ehlers, M.D. (2005). Polarized secretory trafficking directs cargo for asymmetric dendrite growth and morphogenesis. Neuron *48*, 757–771.

Huang, E.J., and Reichardt, L.F. (2003). Trk receptors: roles in neuronal signal transduction. Annu. Rev. Biochem. *72*, 609–642.

Huang, K., and El-Husseini, A. (2005). Modulation of neuronal protein trafficking and function by palmitoylation. Curr. Opin. Neurobiol. *15*, 527–535.

Hudmon, A., and Schulman, H. (2002). Neuronal Ca^{2+}/Calmodulin-dependent protein kinase II: the role of structure and autoregulation in cellular function. Annu. Rev. Biochem. *71*, 473–510.

Jan, Y.-N., and Jan, L.Y. (2003). The control of dendrite development. Neuron *40*, 229–242.

Kawauchi, T., Chihama, K., Nabeshima, Y., and Hoshino, M. (2003). The in vivo roles of STEF/Tiam1, Rac1 and JNK in cortical neuronal migration. EMBO J. *22*, 4190–4201.

Keller, C.A., Yuan, X., Panzanelli, P., Martin, M.L., Alldred, M., Sassoe-Pognetto, M., and Luscher, B. (2004). The gamma2 subunit of $GABA_A$ receptors is a substrate for palmitoylation by GODZ. J. Neurosci. *24*, 5881–5891.

Kennedy, M.B. (2000). Signal-processing machines at the postsynaptic density. Science *290*, 750–754.

Konur, S., and Ghosh, A. (2005). Calcium signaling and the control of dendritic development. Neuron *46*, 401–405.

Kozorovitskiy, Y., Gross, C.G., Kopil, C., Battaglia, L., McBreen, M., Stranahan, A.M., and Gould, E. (2005). Experience induces structural and biochemical changes in the adult primate brain. Proc. Natl. Acad. Sci. USA *102*, 17478–17482.

Kuhn, T.B., Williams, C.V., Dou, P., and Kater, S.B. (1998). Laminin directs growth cone navigation via two temporally and functionally distinct calcium signals. J. Neurosci. *18*, 184–194.

Kumanogoh, H., Miyata, S., Sokawa, Y., and Maekawa, S. (2001). Biochemical and morphological analysis on the localization of Rac1 in neurons. Neurosci. Res. *39*, 189–196.

Linder, M.E., and Deschenes, R.J. (2004). Model organisms lead the way to protein palmitoyltransferases. J. Cell Sci. *117*, 521–526.

Lisman, J., Schulman, H., and Cline, H. (2002). The molecular basis of CaMKII function in synaptic and behavioural memory. Nat. Rev. Neurosci. *3*, 175–190.

Luo, L. (2002). Actin cytoskeleton regulation in neuronal morphogenesis and structural plasticity. Annu. Rev. Cell Dev. Biol. *18*, 601–635.

Matsuo, N., Hoshino, M., Yoshizawa, M., and Nabeshima, Y. (2002). Characterization of STEF, a guanine nucleotide exchange factor for Rac1, required for neurite growth. J. Biol. Chem. *277*, 2860–2868.

Meijering, E., Jacob, M., Sarria, J.C., Steiner, P., Hirling, H., and Unser, M. (2004). Design and validation of a tool for neurite tracing and analysis in fluorescence microscopy images. Cytometry A *58*, 167–176.

Mishina, M., and Sakimura, K. (2007). Conditional gene targeting on the pure C57BL/6 genetic background. Neurosci. Res., in press. Published online January 18, 2007. 10.1016/j.neures.2007.01.004.

Miyoshi, H., Blomer, U., Takahashi, M., Gage, F.H., and Verma, I.M. (1998). Development of a self-inactivating lentivirus vector. J. Virol. *72*, 8150–8157.

Nishimura, H., Sakagami, H., Uezu, A., Fukunaga, K., Watanabe, M., and Kondo, H. (2003). Cloning, characterization and expression of two alternatively splicing isoforms of Ca^{2+}/calmodulin-dependent protein kinase I gamma in the rat brain. J. Neurochem. *85*, 1216–1227.

Ohmae, S., Takemoto-Kimura, S., Okamura, M., Adachi-Morishima, A., Nonaka, M., Fuse, T., Kida, S., Tanji, M., Furuyashiki, T., Arakawa, Y., et al. (2006). Molecular identification and characterization of a family of kinases with homology to Ca2+/calmodulin-dependent protein kinases I/IV. J. Biol. Chem. *281*, 20427–20439.

Pelled, D., Riebeling, C., van Echten-Deckert, G., Sandhoff, K., and Futerman, A.H. (2003). Reduced rates of axonal and dendritic growth in embryonic hippocampal neurones cultured from a mouse model of Sandhoff disease. Neuropathol. Appl. Neurobiol. *29*, 341–349.

Redmond, L., Kashani, A.H., and Ghosh, A. (2002). Calcium regulation of dendritic growth via CaM Kinase IV and CREB-mediated transcription. Neuron *34*, 999–1010.

Schmitt, J.M., Wayman, G.A., Nozaki, N., and Soderling, T.R. (2004). Calcium activation of ERK mediated by calmodulin kinase I. J. Biol. Chem. *279*, 24064–24072.

Schmitt, J.M., Guire, E.S., Saneyoshi, T., and Soderling, T.R. (2005). Calmodulin-dependent kinase kinase/calmodulin kinase I activity gates extracellular-regulated kinase-dependent long-term potentiation. J. Neurosci. *25*, 1281–1290.

Schwarz, A., and Futerman, A.H. (1998). Inhibition of sphingolipid synthesis, but not degradation, alters the rate of dendrite growth in cultured hippocampal neurons. Brain Res. Dev. Brain Res. *108*, 125–130.

Silva, A.J., Kogan, J.H., Frankland, P.W., and Kida, S. (1998). CREB and memory. Annu. Rev. Neurosci. *21*, 127–148.

Soderling, T.R., and Stull, J.T. (2001). Structure and regulation of calcium/calmodulin-dependent protein kinases. Chem. Rev. *101*, 2341–2352.

Suzuki, T., Ito, J., Takagi, H., Saitoh, F., Nawa, H., and Shimizu, H. (2001). Biochemical evidence for localization of AMPA-type glutamate receptor subunits in the dendritic raft. Brain Res. Mol. Brain Res. *89*, 20–28.

Suzuki, S., Numakawa, T., Shimazu, K., Koshimizu, H., Hara, T., Hatanaka, H., Mei, L., Lu, B., and Kojima, M. (2004). BDNF-induced recruitment of TrkB receptor into neuronal lipid rafts: roles in synaptic modulation. J. Cell Biol. *167*, 1205–1215.

Takemoto-Kimura, S., Terai, H., Takamoto, M., Ohmae, S., Kikumura, S., Segi, E., Arakawa, Y., Furuyashiki, T., Narumiya, S., and Bito, H. (2003). Molecular cloning and characterization of CLICK-III/CaMKIgamma, a novel membrane-anchored neuronal Ca^{2+}/calmodulin-dependent protein kinase (CaMK). J. Biol. Chem. *278*, 18597–18605.

Tolias, K.F., Bikoff, J.B., Burette, A., Paradis, S., Harrar, D., Tavazoie, S., Weinberg, R.J., and Greenberg, M.E. (2005). The Rac1-GEF Tiam1 couples the NMDA receptor to the activity-dependent development of dendritic arbors and spines. Neuron *45*, 525–538.

Uemura, T., Mori, H., and Mishina, M. (2002). Isolation and characterization of Golgi apparatus-specific GODZ with the DHHC zinc finger domain. Biochem. Biophys. Res. Commun. *296*, 492–496.

Vaillant, A.R., Zanassi, P., Walsh, G.S., Aumont, A., Alonso, A., and Miller, F.D. (2002). Signaling mechanisms underlying reversible, activity-dependent dendrite formation. Neuron *34*, 985–998.

Van Aelst, L., and Cline, H.T. (2004). Rho GTPases and activity-dependent dendrite development. Curr. Opin. Neurobiol. *14*, 297–304.

Wassif, C.A., Zhu, P., Kratz, L., Krakowiak, P.A., Battaile, K.P., Weight, F.F., Grinberg, A., Steiner, R.D., Nwokoro, N.A., Kelley, R.I., et al. (2001). Biochemical, phenotypic and neurophysiological characterization of a genetic mouse model of RSH/Smith-Lemli-Opitz syndrome. Hum. Mol. Genet. *10*, 555–564.

Wayman, G.A., Kaech, S., Grant, W.F., Davare, M., Impey, S., Tokumitsu, H., Nozaki, N., Banker, G., and Soderling, T.R. (2004). Regulation of axonal extension and growth cone motility by calmodulin-dependent protein kinase I. J. Neurosci. *24*, 3786–3794.

Wayman, G.A., Impey, S., Marks, D., Saneyoshi, T., Grant, W.F., Derkach, V., and Soderling, T.R. (2006). Activity-dependent dendritic arborization mediated by CaM-kinase I activation and enhanced CREB-dependent transcription of Wnt-2. Neuron *50*, 897–909.

Whitford, K.L., Dijkhuizen, P., Polleux, F., and Ghosh, A. (2002). Molecular control of cortical dendrite developement. Annu. Rev. Neurosci. *25*, 127–149.

Wu, G.-Y., and Cline, H.T. (1998). Stabilization of dendritic arbor structure in vivo by CaMKII. Science *279*, 222–226.

Yu, X., and Malenka, R.C. (2003). Beta-catenin is critical for dendritic morphogenesis. Nat. Neurosci. *6*, 1169–1177.

Zacharias, D.A., Violin, J.D., Newton, A.C., and Tsien, R.Y. (2002). Partitioning of lipid-modified monomeric GFPs into membrane microdomains of live cells. Science *296*, 913–916.

Zheng, J.Q., Felder, M., Connor, J.A., and Poo, M.M. (1994). Turning of nerve growth cones induced by neurotransmitters. Nature *368*, 140–144.

Neuron, Volume *54*

Supplemental Data

Regulation of Dendritogenesis via a Lipid-Raft-Associated Ca^{2+}/Calmodulin-Dependent Protein Kinase CLICK-III/CaMKIγ

Sayaka Takemoto-Kimura, Natsumi Ageta-Ishihara, Mio Nonaka, Aki Adachi-Morishima, Tatsuo Mano, Michiko Okamura, Hajime Fujii, Toshimitsu Fuse, Mikio Hoshino, Shingo Suzuki, Masami Kojima, Masayoshi Mishina, Hiroyuki Okuno, and Haruhiko Bito

Experimental Procedures:

Cloning and plasmid constructions

Mouse CLICK-III (CL3) /CaMKIγ cDNA (Takemoto-Kimura et al., 2003) was inserted into pEGFPC1 vector (BD Clontech) to generate pEGFP-CL3. The expression vectors for C-to-S mutants, pEGFP-CL3C474S, -C466S, -C435S, -C423S, -C417/419/420S, -C392S, -C375S and a quadruple substitution mutant pEGFP-CL34CS (C417, 419, 420, 423S) were created from pEGFP-CL3 by stepwise substitution of each Cys codon into a Ser codon. A lysine (amino acid residue 52)-to-alanine mutation was introduced by site-directed mutagenesis to generate pEGFP-CL3K52A. The EGFP-CL3 fragments were transferred into pMCS-CAG vector (identical to pcCAG as described by Kawauchi et al., 2003) to create pCAG-EGFP-CL3 and pCAG-EGFP-CL3K52A. YFP- and CFP-tagged CL3 were generated by replacing the EGFP moiety of pEGFP-CL3 with either Venus (a kind gift from Dr. Atsushi Miyawaki, RIKEN-BSI, Japan) (Nagai et al., 2002) or Cerulean (Rizzo et al., 2004), which are improved versions of YFP and CFP, respectively. pcDNA3-HA-CL3C474S and pcDNA3-HA-CL34CS were created from pcDNA3-HA-CL3

(Takemoto-Kimura et al., 2003).

Short hairpin RNA vectors were constructed based upon a modified version of pSUPER vector, pSUPERneo+GFP (OligoEngine) or pSUPER+mRFP1, in which a short hairpin RNA and either a fluorescent marker GFP or mRFP1 (a kind gift from Dr. Roger Tsien, UCSD and HHMI) (Campbell et al., 2002) were dually expressed under the H1 promoter and the PGK promoter, respectively. To create pSUPER-shCL3, pSUPER-shCaMKIIα, and pSUPER-shCaMKIV, two complementary 60-bp oligonucleotides carrying antisense and sense sequences for GAAACAGACCACCAACATC (19-bp, corresponding to nucletides 39-57 of mouse CL3), GGATCTGATCAATAAGATG (nucleotides 735-753 of mouse CaMKIIα) and GTGTTAAAGAAAACAGTGG (nucleotides 214-232 of mouse CaMKIV) were annealed and ligated to pSUPER vectors in accordance with OligoEngine's instructions. pSUPER-shNega was generated similarly except that an artificial 19-mer sequence (ATCCGCGCGATAGTACGTA) was used as a target. This sequence was based upon a commercially available negative control siRNA sequence (B-Bridge International), and we confirmed it had no significant identity to any known mammalian gene based on a BLAST search. The specificity of the CL3 shRNA vector against other CaMKs was tested using CL3 shRNA expressing hippocampal neurons (>15DIV) and immunoreactivity against CaMKIIα, CaMKIIβ and CaMKIV was shown to be unaltered. For the rescue experiments, three silent mutations were introduced into the shRNA target sequence of EGFP-tagged wildtype and mutant CL3 to generate shRNA-resistant cDNAs (pEGFP-$CL3_{res}$ and related constructs) and the open reading frames were further transferred into pCAG-MCS vector. All mutated regions for CL3 vectors were verified by sequencing.

pmCherry-β-actin was created by essentially replacing the EGFP moiety of pEGFP-β-actin (Furuyashiki et al., 2002) with mCherry (a kind gift from Dr. Roger Tsien,

UCSD and HHMI) (Shaner et al., 2004). GODZ cDNA (Uemura et al., 2002) was subcloned into pcDNA3-HA (Takemoto-Kimura et al., 2003). pEGFP-V12Rac1 was generated by site-directed mutagenesis from pEGFP-N17Rac1 (a kind gift from Dr. Shuh Narumiya, Kyoto University, Japan) and pcDNA3-Flag-PHnTSS STEF was as described (Matsuo et al., 2002). Lyn-CFP was obtained by fusing a C-terminal Myc-tag of an active Lyn-Myc (a generous gift from Dr. Zen-ichiro Honda, Department of Allergy and Rheumatology, the University of Tokyo Hospital, Japan) in-frame with Cerulean. EGFP-GluR1 was created from mouse GluR1 (Sakimura et al. 1990) according to Shi et al. (1999). MAP2-CTF-RFP was a kind gift from Dr. Fumitaka Oyama (RIKEN Brain Science Institute, Wako, Japan) and Yasuo Ihara (University of Tokyo Graduate School of Medicine, Tokyo, Japan).

Immunocytochemistry

Primary antibodies used were mouse anti-HA, rat anti-HA (Roche Diagnostics), mouse anti-HA (Cell Signaling), mouse anti-FLAG (Sigma), mouse anti-GM130 (BD Transduction Laboratories), rabbit anti-DsRed (BD Clontech), mouse anti-Tau-1, rabbit anti-microtubule-associated protein 2 (MAP2) (Chemicon). For secondary fluorescent detection, Alexa 405-, Alexa 488-, Alexa 555-, Alexa 594- conjugated anti-mouse, anti-rabbit, and anti-rat IgG antibodies (Molecular Probes) were employed. Wide-field fluorescent images were obtained using a 20x (UplanFL 20x/NA 0.5, air, Olympus, Japan), a 40x (UplanFL 40x/NA 0.75 air, Olympus) or a 100x objective (UplanApo 100x NA 1.35 oil, Olympus) in combination with either a color CCD camera (DP-70, Olympus) on an upright microscope (BX-51, Olympus), or an EM-CCD camera (iXon, Andor) on an inverted microscope (IX-81, Olympus). Confocal fluorescent images were taken by a confocal laser microscopy system (LSM 510META-V3.2, Carl Zeiss) built on an inverted microscope

(Axiovert 200M, Carl Zeiss) with 63x or 40x objectives (Plan-Apochromat 63x/NA 1.4, oil, Plan-Neofluar 40x/NA 1.3, oil, Carl Zeiss). In most cases, projected images of confocal sections were shown, but occasionally, for clear separation of membrane- and/or Golgi-fluorescent signals, single confocal sections were shown (Fig. 3E-H, Suppl. Figs. 1A, 7A, 8B).

Calcium imaging

Twenty-four hours after plating, cortical neurons on glass-bottom dishes were loaded with Fluo-4/AM (2.5 μM, Dojindo laboratories, Kumamoto, Japan) for 30 min at room temperature. After wash, cells were incubated at 37 °C in a stage CO_2 chamber (Tokai Hit Co., Ltd, Shizuoka, Japan) equipped on an Olympus IX81 inverted microscope. Time-lapse fluorescence images were recorded at 4 frames/sec through a 40 x objective (NA 1.35) using an EM-CCD camera (Hamamatsu Photonics, Hamamatsu, Japan) driven by an imaging software (Aquacosmos Ver. 2.6, Hamamatsu Photonics). Culture medium was continuously perfused during imaging session using a peristaltic pump (Rainin Instrument, Woburn, MA). After baseline recording, a medium containing BDNF (50 ng/ml) was bath-applied through the pump. Fluorescence changes in the cell bodies of individual cells were analyzed using the Metamorph or Image J software, and raw pixel fluorescence values were normalized with those in the first image (F/Fo). A majority of cells (83% ± 9.9, mean ± s.d.) showed BDNF-induced calcium mobilization in our culture (N = 5 independent dishes).

Rac1 pulldown assays

For Rac1 pulldown assays, cortical neurons were electroporated with pSUPER vectors by Nucleofector and plated onto poly-D-Lysine-coated 6-cm dishes at the density of

3.8 x $10^5/cm^2$ and then harvested at 2 DIV. Cells were washed once in ice-cold PBS(-) and lysed in the lysis buffer containing 25mM Tris-HCl (pH 7.5), 150 mM NaCl, 5 mM $MgCl_2$, 1% NP-40, 1 mM DTT, 5% glycerol, and a Complete EDTA-free protease inhibitor cocktail. The lysates were centrifuged at 16,000 g for 15 min at 4°C, and the supernatant was collected. The protein concentrations were determined using a BCA Protein Assay Reagent kit (Pierce). GTP-bound activated Rac1 was detected by a pulldown assay using an EZ-detect Rac1 activation kit (Pierce), according to the manufacturer's protocol. Briefly, SwellGel-immobilized gluthatione discs were placed into spin columns together with 20 μg of GST-human Pak1-PBD and cell lysates containing at least 1 mg of proteins. The reaction mixtures were incubated for 1 h at 4°C with gentle rocking. The resin was washed three times in the lysis buffer followed by addition of 50 μl of 2X SDS sample buffer and by boiling for 5 min. The eluted fractions were collected and subjected to SDS-PAGE and Western blot analysis. ECL reaction time and film exposure times were adjusted to maintain the signals within a linear dynamic range of detection.

Measurement of fluorescence resonance energy transfer

For FRET experiments, cultured rat hippocampal neurons were prepared on Matrigel-coated glass bottom dishes (MatTek Corporation). Neurons were transfected with a mixture of CFP- and YFP-CL3 at a ratio of 1:4 using Lipofectamine 2000 at 12-17 DIV. Images were taken from living neurons 2-4 days after the transfection, using the LSM 510META confocal microscope equipped with a heated stage CO_2 incubator (Tokai Hit, Japan). FRET was measured by the donor (CFP) dequenching after acceptor (YFP) photobleaching method. CFP and YFP signals were monitored by independent scans using a 458 nm- and a 514 nm-laser for excitation, coupled with 470-500 nm (for CFP) and 530-600

nm (for YFP) band-pass filters, respectively. The acceptor photobleaching was achieved with repetitive scans with intense 514 nm-laser light on the cell body as well as dendritic regions of transfected neurons, with no detectable photodamage. On average, 85 ± 11% (mean ± SD) of YFP signals were specifically bleached after one photobleaching session. Region of interests for quantification were set on neuronal cell bodies in the present study. After background subtraction, FRET efficiency was calculated from CFP signals, before and after the YFP photobleaching, according to a following formula:

FRET efficiency (%) = $(F_{CFP, after} - F_{CFP, before}) \times 100/F_{CFP, after}$

Where $F_{CFP, before}$ and $F_{CFP, after}$ represent the CFP fluorescence signals before and after the acceptor photobleaching.

Quantification of Golgi deformation

In experiments described in Suppl. Fig. 7, hippocampal neurons were transfected at 7 DIV with pSUPER vectors as described above and then fixed at 9 DIV. Stacks of confocal images (at 0.9 μm z-interval / section) were acquired to image GM130 immunopositive signals for each neuron, and a single confocal section that contained the highest integrated fluorescence intensity for GM130 immunoreactivity was selected. After background subtraction, a cutoff threshold of 1/4 of maximal GM130 intensity was used as a criterion to define a Golgi region that was positive for GM130 immunoreactivity. A CL3 knockdown neuron typically contained a comparable amount of GM130-positive pixels, but showed a more disassembled pattern of Golgi region consisting of an increased number of smaller patches. The total area and the number of individual Golgi regions were determined by Metamorph software.

Additional References for Supplementary Materials:

Campbell, R. E., Tour, O., Palmer, A. E., Steinbach, P. A., Baird, G. S., Zacharias, D. A., and Tsien, R. Y. (2002). A monomeric red fluorescent protein. Proc. Natl. Acad. Sci. U. S. A. *99*, 7877-7882.

Nagai, T., Ibata, K., Park, E. S., Kubota, M., Mikoshiba, K., and Miyawaki, A. (2002). A variant of yellow fluorescent protein with fast and efficient maturation for cell-biological applications. Nat. Biotechnol. *20*, 87-90.

Rizzo, M. A., Springer, G. H., Granada, B., and Piston, D. W. (2004). An improved cyan fluorescent protein variant useful for FRET. Nat. Biotechnol. *22*, 445-449.

Sakimura, K., Bujo, H., Kushiya, E., Araki, K., Yamazaki, M., Yamazaki, M., Meguro, H., Warashina, A., Numa, S., and Mishina, M. (1990). Functional expression from cloned cDNAs of glutamate receptor species responsive to kainate and quisqualate.
FEBS Lett. *272*, 73-80.

Shaner, N. C., Campbell, R. E., Steinbach, P. A., Giepmans, B. N., Palmer, A. E., and Tsien, R. Y. (2004). Improved monomeric red, orange and yellow fluorescent proteins derived from Discosoma sp. red fluorescent protein. Nat. Biotechnol. *22*, 1567-1572.

Shi, S. H, Hayashi, Y., Petralia, R. S, Zaman, S. H, Wenthold, R. J, Svoboda, K., and Malinow, R. (1999). Rapid spine delivery and redistribution of AMPA receptors after synaptic NMDA receptor activation. Science *284*, 1811-1816.